Wannier interpolation scheme for phonon-induced potentials: Application to bulk MgB$_2$, W, and the (1×1) H-covered W(110) surface

Asier Eiguren[1,2] and Claudia Ambrosch-Draxl[1]

[1]*Chair of Atomistic Modelling and Design of Materials, University of Leoben, Franz-Josef-Straße 18, A-8700 Leoben, Austria*
[2]*Donostia International Physics Center (DIPC), Paseo Manuel de Lardizabal 4, 20018 Donostia/San Sebastian, Spain*

We present an efficient scheme for calculating phonon-induced potentials with high precision. The method exploits the idea of Wannier functions applied to the change of the electron potentials, allowing for an accurate evaluation of coupling constants for arbitrary wave vectors. In order to demonstrate the capability of the method, we include three examples: bulk MgB$_2$, bcc tungsten, and the hydrogen covered 1 × 1 W(110) surface. For these cases we calculate the momentum resolved (**k** dependent) Eliashberg function for a selected set of **k** points and the electron-phonon mass enhancement parameter $\lambda_\mathbf{k}$.

I. INTRODUCTION

Lattice vibrations represent low energy collective excitations in solids that can dramatically affect the quasiparticle states close to the Fermi surface. The most striking example is the phonon-induced superconducting transition. Moreover, phonon-scattering processes lead to a pronounced reduction in the quasiparticle lifetimes as well as to a characteristic modulation of the quasiparticle dispersion due to virtual emission of phonon modes at low temperatures. These effects are measurable by various experimental probes, including direct photoemission,[1–6] cyclotron,[7] or thermodynamic measurements.[8] Both the altered lifetime and the change in the quasiparticle velocity have an impact on the low energy dynamical properties of a material. This can be particularly important in systems with reduced dimensionality where the electron-phonon (*ep*) interaction is typically stronger than in the three-dimensional (3D) environment. At the same time, low-dimensional systems are most relevant in the emerging field of nanotechnology and nanodevices. Thus a very good understanding of the *ep* interaction is of great importance especially for problems related to charge transport properties.

The *ep* mass enhancement parameter $\lambda_\mathbf{k}$ and the Eliashberg function $\alpha^2 F_{i,\mathbf{k}}(\omega)$ are among the most meaningful quantities describing *ep* effects in metals. They reflect the strength of the *ep* interaction and allow the determination of many other related quantities, including the *ep* contribution to the superconducting gap (through Eliashberg theory), the heat capacity, or some transport properties.[8,9] Much of the current effort from the theoretical point of view is concentrated on calculating the electron momentum resolved $\alpha^2 F_{i,\mathbf{k}}(\omega)$ in bulk and/or surface systems.

The most demanding part in the calculation of vibrational or electron-phonon related properties is the self-consistent determination of the phonon-induced change of the electron potential. State of the art first-principles methods include supercell approaches or the more efficient perturbative linear-response technique. In any case, for systems including several atoms, even linear-response calculations can hamper a highly precise calculation of anisotropic (**k** dependent) *ep* properties. In such cases, the high computational effort makes it virtually impossible to determine the *ep* matrix el-

ements for **q** point samplings denser than ∼20 × 20 × 20. To overcome this obstacle is one of the main objectives of this work.

Savrasov and Savrasov[10] partially solved the problem by considering coarse phonon grids with a much denser division for electron wave vectors (e.g., an 8 × 8 × 8 **q** grid and a 32 × 32 × 32 **k** mesh, respectively). This procedure gives reasonably accurate Eliashberg functions averaged over the Fermi surface due to cancellation of errors. However, calculating the momentum resolved Eliashberg function for such a sampling still leads to poor results for each particular function. In other words, if the objective is to accurately obtain the anisotropy of the Eliashberg function, a dense momentum sampling is needed not only for the electron wave functions but also for the phonons.

Choi *et al.*[11] developed a method to interpolate the variation of the electron potential by first performing a self-consistent phonon calculation in high-symmetry points and inferring the potential for arbitrary momentum by an (unspecified) interpolation technique. They applied this method to bulk MgB$_2$ to obtain the electron-phonon mass enhancement parameter at the Fermi surface.

Giustino and co-workers[12,13] have very recently developed a promising scheme to calculate *ep* matrix elements in very densely sampled Brillouin zones (BZs). This method takes advantage of the localization properties of both the maximally localized electron Wannier functions[14] and similarly defined Wannier functions for phonons. The interpolation technique is made efficient by considering the localization of the Wannier functions and neglecting their overlaps at some distance in real space. In essence, this method interpolates electron wave functions, phonon modes, and phonon-induced potentials on the same footing. It has also been applied to obtain the self-energy of graphene.[15]

In this work, we present an approach in which the local part of the potential changes and dynamical matrices are Fourier interpolated but all the electron wave functions are calculated directly from the self-consistent potential. This procedure allows us to efficiently determine the *ep* coupling parameters for arbitrary phonon wave vectors **q** and consequently, the **k** resolved Eliashberg functions. The method is relatively simple and allows for a precision, which, in many

systems, is not accessible by direct calculations due to computational costs. Concerning the solution of the Kohn-Sham equation, we focus here on norm-conserving pseudopotentials where our method is easy to introduce. From the several successful implementations of the linear-response method,[10,16,17] we have used the PWSCF linear-response code in our work. We present results for bulk bcc tungsten and bulk MgB_2 as well as for the complex 1×1 H covered W(110) surface.

II. METHOD

A. Theory background

Within the quasielastic approximation, the electron momentum (**k**) resolved Eliashberg function is defined as

$$\alpha^2 F_{i,\mathbf{k}}(\omega) = \sum_{\mathbf{q},\nu}^{j} |g_{\mathbf{k},\mathbf{k}-\mathbf{q}}^{j,\nu}|^2 \delta(\omega - \omega_\mathbf{q}) \delta(\epsilon_\mathbf{k} - \epsilon_{\mathbf{k}-\mathbf{q}}), \quad (1)$$

where i is the electron band index, and ν and **q** denote the phonon mode and its wave vector, respectively. The summation runs over the final electron states j with wave vectors **k**−**q**. The *ep* matrix element $g_{\nu,\mathbf{k},\mathbf{k}-\mathbf{q}}^{i,j}$ is given by

$$g_{\nu,\mathbf{k},\mathbf{k}-\mathbf{q}}^{i,j} = \sum_{s,\alpha} \frac{\epsilon_{s,\alpha}^{\mathbf{q},\nu}}{\sqrt{2M_s \omega_\mathbf{q}^\nu}} \langle \psi_{j,\mathbf{k}-\mathbf{q}} | \delta_\mathbf{q}^{s,\alpha} V | \psi_{i,\mathbf{k}} \rangle, \quad (2)$$

where $s=1, \ldots, N$ labels the atomic sites inside a particular unit cell, $\alpha=1,2,3$ refers to the three Cartesian coordinates, and $\epsilon_{s,\alpha}^{\mathbf{q},\nu}$ represents the polarization vector of the phonon mode ν. $\delta_\mathbf{q}^{s,\alpha} V$ is the self-consistent variation of the effective potential due to a frozen-in displacement of atom s in direction α. The relation between $\lambda_{i,\mathbf{k}}$ and the Eliashberg function is given by

$$\lambda_{i,\mathbf{k}} = 2 \int \alpha^2 F_{i,\mathbf{k}}(\omega)/\omega d\omega. \quad (3)$$

$\lambda_\mathbf{k}$ directly determines the low-temperature quasiparticle mass enhancement close to the Fermi level (ϵ_F) where the velocity is reduced according to $\mathbf{v}_\mathbf{k} \simeq \mathbf{v}_\mathbf{k}^0/(1+\lambda_\mathbf{k})$. The electron lifetime broadening at high temperatures, $\Gamma_\mathbf{k} \approx 2\pi T \lambda_\mathbf{k}$, is also proportional to $\lambda_\mathbf{k}$.

The most serious difficulty when calculating the Fermi-surface integrals involved in Eq. (1) is the accurate evaluation of the large amount of *ep* matrix elements $g_{\nu,\mathbf{k},\mathbf{k}-\mathbf{q}}^{i,j}$ needed to sample the Fermi surface. The first step in such a calculation is an accurate determination of the phonon band structure, which is briefly outlined in the following.

The linear-response scheme is based on the solution of the Sternheimer equation

$$[H(\mathbf{r}) - \epsilon_{\mathbf{k},i}]\delta_\mathbf{q}^{s,\alpha} \psi_\mathbf{k}(\mathbf{r}) = [\delta_\mathbf{q}^{s,\alpha} V(\mathbf{r}) - \delta_\mathbf{q}^{s,\alpha} \epsilon_{\mathbf{k},i}]\psi_\mathbf{k}(\mathbf{r}), \quad (4)$$

where the first-order change in the potential consists of contributions from the Hartree part, V_H, the exchange-correlation potential, V_{xc}, and the bare pseudopotential, V_b, respectively:

$$\delta_\mathbf{q}^{s,\alpha} V(\mathbf{r},\mathbf{r}') \equiv \delta_\mathbf{q}^{s,\alpha} V_H(\mathbf{r}) + \delta_\mathbf{q}^{s,\alpha} V_{xc}(\mathbf{r}) + \delta_\mathbf{q}^{s,\alpha} V_b(\mathbf{r},\mathbf{r}'). \quad (5)$$

The solution of Eq. (4) is very well documented in literature.[10,16–18] The relevant input is the variation of the bare pseudopotential $\delta_\mathbf{q}^{s,\alpha} V_b(\mathbf{r},\mathbf{r}')$ while the output comprises the first-order changes in the potential, the wave functions, and the density. In the first step of the self-consistency process, the variation of the electron wave functions $\delta_\mathbf{q}^{s,\alpha} \psi_\mathbf{k}(\mathbf{r})$ is calculated, allowing the evaluation of the total change in the electron charge density. In the next step, the variation of the Hartree and *xc* potentials, $\delta_\mathbf{q}^{s,\alpha} V_H(\mathbf{r})$ and $\delta_\mathbf{q}^{s,\alpha} V_{xc}(\mathbf{r})$, are updated,[10,16] and the process is repeated until a self-consistent $\delta_\mathbf{q}^{s,\alpha} V$ is obtained.

These calculations are usually performed for a discrete set of frozen-in perturbations with wave vector **q** sampling the irreducible wedge of the BZ. For a given **q**, one should in general take into account $3N$ different displacements $\delta_\mathbf{q}^{s,\alpha}$. However, symmetry considerations allow the reduction in the amount of patterns to be calculated for some particular (higher symmetry) **q** points.

B. Wannier-function based interpolation technique

An atomic displacement implies a perturbation where the induced potential $\delta_\mathbf{q}^{s,\alpha} V_{ind}(\mathbf{r})$, consisting of Hartree and *xc* contribution

$$\delta_\mathbf{q}^{s,\alpha} V_{ind}(\mathbf{r}) \equiv \delta_\mathbf{q}^{s,\alpha} V_H(\mathbf{r}) + \delta_\mathbf{q}^{s,\alpha} V_{xc}(\mathbf{r}), \quad (6)$$

together with the bare perturbation $\delta_\mathbf{q}^{s,\alpha} V_b(\mathbf{r},\mathbf{r}')$, represents the total change of the potential. While the bare part of the potential has a local and a nonlocal component,[16]

$$\delta_\mathbf{q}^{s,\alpha} V_b(\mathbf{r},\mathbf{r}') \equiv \delta_\mathbf{q}^{s,\alpha} V_{b,l}(\mathbf{r})\delta(\mathbf{r}-\mathbf{r}') + \delta_\mathbf{q}^{s,\alpha} V_{b,nl}(\mathbf{r},\mathbf{r}'), \quad (7)$$

the induced part is purely local. The local part of the total change of the electron potential is given by

$$\delta_\mathbf{q}^{s,\alpha} V_l(\mathbf{r}) \equiv \delta_\mathbf{q}^{s,\alpha} V_{b,l}(\mathbf{r}) + \delta_\mathbf{q}^{s,\alpha} V_{ind}(\mathbf{r}). \quad (8)$$

This quantity is computationally demanding and hence needs to be interpolated while the calculation of $\delta_\mathbf{q}^{s,\alpha} V_b(\mathbf{r},\mathbf{r}')$ hardly requires any computing time since it is simply obtained from the gradient of the pseudopotential. Our technique is based on the observation that this local part of the phonon-induced potential [Eq. (8)] has a quite smooth dependence on **q**.

Let us suppose that $\delta_\mathbf{q}^{s,\alpha} V_l(\mathbf{r})$ has been calculated self-consistently for a regular but relatively coarse **q** grid of the entire Brillouin zone. In practice, this is done by applying the appropriate symmetry operations to the potentials calculated for the irreducible **q** set. Since $\delta_\mathbf{q}^{s,\alpha} V(\mathbf{r})$ is periodic in momentum space, $\delta^{\mathbf{q}+\mathbf{G},\nu} V(\mathbf{r}) = \delta^{\mathbf{q},\nu} V(\mathbf{r})$. One can then perform the Fourier transform of $\delta^{\mathbf{q},\nu} V(\mathbf{r})$, obtaining the potential counterpart of the electron Wannier function,

$$W_l^{s,\alpha}(\mathbf{r} - \mathbf{R}) \equiv \sum_\mathbf{q} \delta_\mathbf{q}^{s,\alpha} V_l(\mathbf{r}) e^{i\mathbf{R}\mathbf{q}}. \quad (9)$$

$W_l^{s,\alpha}(\mathbf{r}-\mathbf{R})$ is a localized function and represents the variation of the induced part of the potential due to the displacement of a single atom s in the Cartesian direction α. This function can be used to obtain the change of the potential for an arbitrary wave vector $\tilde{\mathbf{q}}$ by considering the inverse Fourier transformation of $W_l^{s,\alpha}(\mathbf{r}-\mathbf{R})$:

$$\delta_{\tilde{\mathbf{q}}}^{s,\alpha} V_l(\mathbf{r}) \simeq \sum_{\mathbf{R}} W_l^{s,\alpha}(\mathbf{r} - \mathbf{R}) e^{-i\mathbf{R}\tilde{\mathbf{q}}}. \qquad (10)$$

The more localized the potential change Wannier function is, the more accurate is the potential approximated by this scheme.

All this is very similar to what is found for electron Wannier functions.[14] However, note that contrary to the electronic case, the phases of $\delta_{\mathbf{q}}^{s,\alpha} V_l(\mathbf{r})$ are fixed since this is the case for the bare part of the potential. Thus Eq. (9) already represents a maximally localized Wannier potential for a single band. Still, in allowing for band mixing, one would obtain even more localized potential Wannier functions in the same way as for the electronic case[14] with the only drawback of slightly complicating the computational procedure. Of course, the accuracy of the above interpolation technique also depends on the density of the original $\mathbf{q}$ mesh. The experience gained by applying this procedure to several systems, however, has revealed that even starting with relatively coarse $\mathbf{q}$ grids (of the order of $\sim 8 \times 8 \times 8$) gives accurate results for the anisotropic *ep* properties.

Our method is summarized as follows: As a first step, one performs a self-consistent linear-response calculation for a relatively coarse phonon $\mathbf{q}$ sampling to get the dynamical matrices $D_{\mathbf{q}}(s, \alpha; s', \alpha')$ and the change of the potentials $[\delta_{\tilde{\mathbf{q}}}^{s,\alpha} V(\mathbf{r})]$ in the irreducible wedge of the Brillouin zone. In a next step, these quantities are calculated for the entire Brillouin zone by considering the appropriate symmetry operations. With these ingredients, one can solve Eqs. (9) and (10) to obtain the change of the potentials for a dense $\mathbf{q}$ mesh, i.e., the same as the one considered for the electron wave functions $(N_{k_1}, N_{k_2}, N_{k_3})$. We now can calculate any electron-phonon matrix element,

$$g_{\nu, \mathbf{k}, \mathbf{k}-\tilde{\mathbf{q}}}^{i,j} = \sum_{s,\alpha} \frac{\epsilon_{s,\alpha}^{\tilde{\mathbf{q}},\nu}}{\sqrt{2M_s \omega_{\tilde{\mathbf{q}}}^{\nu}}} \langle \psi_{j,\mathbf{k}-\tilde{\mathbf{q}}} | \delta_{\tilde{\mathbf{q}}}^{s,\alpha} V | \psi_{i,\mathbf{k}} \rangle, \qquad (11)$$

for $\mathbf{k}$ and $\tilde{\mathbf{q}} \in (N_{k_1}, N_{k_2}, N_{k_3})$.

The phonon energies $\omega_{\tilde{\mathbf{q}}}^{\nu}$ and the polarization vectors $\epsilon_{s,\alpha}^{\mathbf{q},\nu}$ are calculated by the following well-known procedure: The force-constant matrices $\Phi_{\mathbf{R}}$ are obtained by Fourier interpolation of the dynamical matrices $D_{\mathbf{q}}$ derived from the self-consistent linear-response calculations,

$$\Phi_{\mathbf{R}}(s, \alpha; s', \alpha') \equiv \sum_{\mathbf{q}} D_{\mathbf{q}}(s, \alpha; s', \alpha') e^{i\mathbf{q}(\mathbf{r}_s - \mathbf{r}_{s'} + \mathbf{R})}. \qquad (12)$$

Thereby $\mathbf{r}_s$ denote different atomic positions in the same unit cell. To obtain the approximate dynamical matrices, an inverse Fourier transform is performed:

$$D_{\tilde{\mathbf{q}}}(s, \alpha; s', \alpha') \simeq \sum_{\mathbf{R}} \Phi_{\mathbf{R}}(s, \alpha; s', \alpha') e^{-i\tilde{\mathbf{q}}(\mathbf{r}_s - \mathbf{r}_{s'} + \mathbf{R})}. \qquad (13)$$

As mentioned before, Giustino and co-workers[12,13] have applied a Fourier interpolation technique involving maximally localized electron and phonon wave functions. Our method is different in many respects but the most important distinction being that, in our case, the only interpolated quantity is the local part of the phonon-induced part of the electron potential. In the presented procedure here, the electron
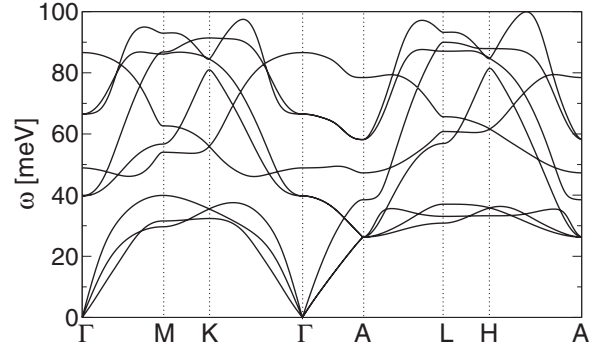

FIG. 1. Phonon band structure of MgB_2 along high-symmetry lines as indicated in Fig. 4.

wave functions and the nonlocal part of the potential are always considered "exactly." This scheme also allows the calculation of the change of the electron potential in real space and hence to solve the Dyson equation for the *ep* problem in real space.[19]

III. RESULTS

A. MgB$_2$

As a first example, we have applied our method to bulk MgB_2 using the experimental structure parameters $a = 5.8317$ and $c/a = 1.1419$.[20,21] We utilized norm conserving pseudopotentials with an energy cutoff of 60 Ry. The ground-state calculations were performed considering a $40 \times 40 \times 40$ grid for the electron wave vector $\mathbf{k}$, labeled G_{40} in the following. The Sternheimer equation was solved for a set of 84 irreducible phonon wave vectors $\mathbf{q}$ representing a $10 \times 10 \times 10$ division of the BZ and considering a G_{20} electron momentum grid for each $\mathbf{q}$ point in the Sternheimer equation. Figure 1 shows the phonon dispersion calculated by means of force-constant matrices obtained from the self-consistently evaluated initial G_{10} $\mathbf{q}$ mesh. It is in very good agreement with previous calculations[22,23] performed for somewhat coarser $(6 \times 6 \times 6)$ $\mathbf{q}$ grids. As a next step, we determined the Eliashberg function considering the three different grids, i.e., G_{10}, G_{20}, and G_{40}, for the electronic wave functions. For the denser $\mathbf{k}$ and $\mathbf{q}$ grids, $(G_{20}$ and $G_{40})$, we computed $\delta_{\mathbf{q}}^{s,\alpha} V(\mathbf{r})$ for irreducible $\mathbf{q}$ points and calculated the potential changes for the full BZ by applying the corresponding symmetry operations. That way we obtained the $\mathbf{k}$ resolved Eliashberg function [Eq. (1)] as well as the Fermi-surface averaged Eliashberg function,

$$\alpha^2 F_{av}(\omega) = \sum_{\mathbf{k},i} \alpha^2 F_{i,\mathbf{k}}(\omega) \delta(\epsilon_{i,\mathbf{k}} - \epsilon_F)/N(0). \qquad (14)$$

The Fermi-surface integrals in Eqs. (1) and (14) where performed using the linear tetrahedron method. The Eliashberg function for some selected directions on the different Fermi sheets, i.e., σ_1, σ_2, π_1, and π_2, are displayed in Fig. 2. These $\mathbf{k}$ directions correspond to the intersections of the Fermi surface with the respective high-symmetry lines indicated in the different panels of the figure. Also, the Eliashberg function averaged over the Fermi surface [Eq. (14)] is shown in Fig. 3 for the different BZ samplings.
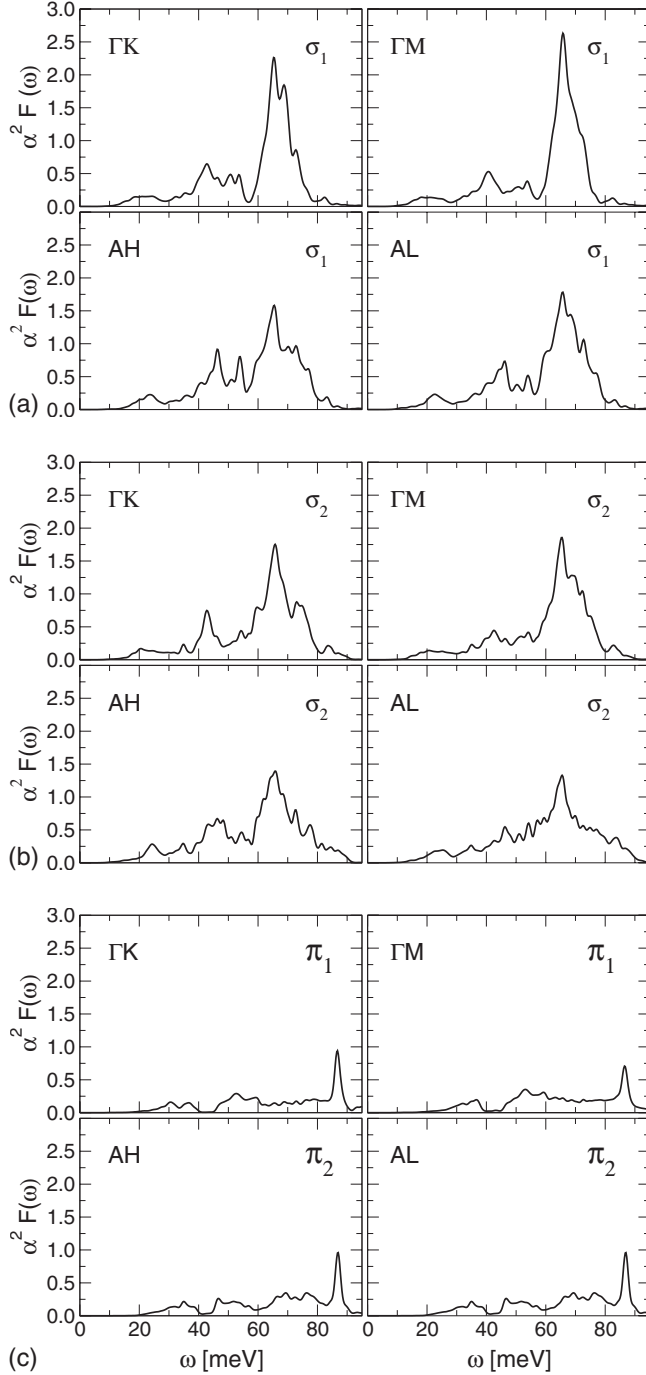
(a)
(b)
(c)

FIG. 2. Eliashberg function on the different Fermi sheets for selected directions as indicated in Fig. 4.
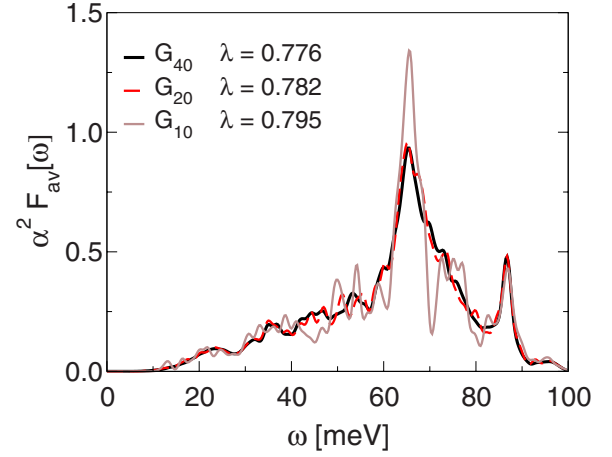

FIG. 3. (Color online) Fermi-surface averaged Eliashberg function considering a $10 \times 10 \times 10$ (G_{10}), $20 \times 20 \times 20$ (G_{20}), and $40 \times 40 \times 40$ (G_{40}) grid for both electron and phonon wave vectors, **k** and **q**.

Note that these calculations are performed with many more **q** and **k** points than in any previous work where the different results for the averaged λ parameter range between 0.7–0.9.[22,24,25] Our converged result for the averaged mass enhancement parameter is $\lambda = 0.776$, where we have used a $40 \times 40 \times 40$ grid for both the electrons and the phonons.

In order to estimate the error in our procedure, we solved the Sternheimer equation self-consistently for some **q** points belonging to G_{20} but not to G_{10}, and then compared the difference between our interpolated potentials (out of an initial G_{10} grid) and the self-consistently obtained ones. This was done starting from the Γ point and going along the three reciprocal-lattice vectors. This is the most stringent test of our method since, close to the Γ point, the response function diverges (as well as the bare potential) and hence the area close to Γ is most sensitive.

The maximum estimated error

$$\epsilon \simeq \frac{\int d^3\mathbf{r} \, |\delta_{\mathbf{q}}^{s,\alpha} V_{\text{loc}}^{ip}(\mathbf{r}) - \delta_{\mathbf{q}}^{s,\alpha} V_{\text{loc}}^{\text{exact}}(\mathbf{r})|}{\int d^3\mathbf{r} \, |\delta_{\mathbf{q}}^{s,\alpha} V_{\text{loc}}^{\text{exact}}(\mathbf{r})|}, \qquad (15)$$

with *ip* indicating the interpolated potential, was always less than 0.1% for the Mg displacements and <1% for the B displacement modes. For **q** points inside the Brillouin zone, the results of the interpolation are even much more accurate. Note that the error estimation given above is rather pessimistic since, in accumulating all errors point per point (by summing over the module of the difference), Eq. (15) does not allow for any error cancellation and hence represents the worst case scenario.

B. Bulk tungsten

As a second example, we considered bcc tungsten (lattice parameter $a = 5.90$ a.u.). A cut-off energy of 40 Ry was used for the ground state as well as for the self-consistent linear-response calculations. The latter was performed for a G_8
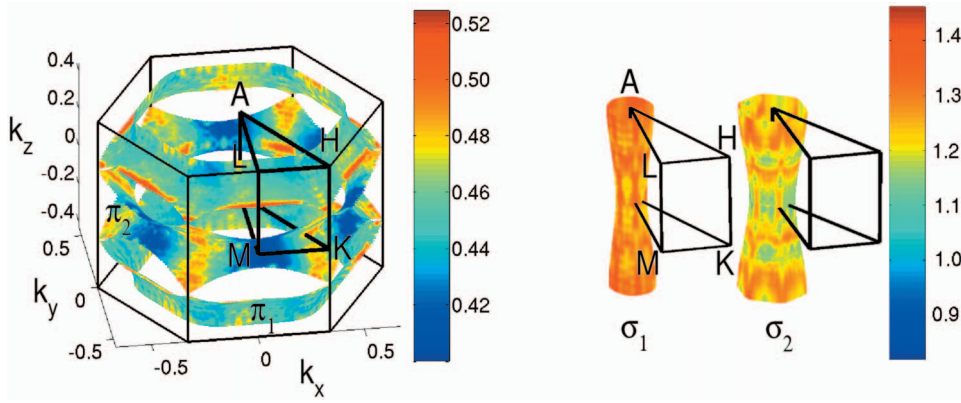
Figure 4 shows the Fermi surface of bulk MgB$_2$ where the calculated values of the *ep* parameter $\lambda_{\mathbf{k}}$ are highlighted by the color code. The two central cylindrical sheets are labeled by σ_1 and σ_2, and the outer ones as π_1 and π_2, indicating the corresponding band character. Note that $\lambda_{\mathbf{k}}$ is rather isotropic for the π bands, contrary to the σ type sheets where not only is the magnitude twice as large but also the anisotropy is more pronounced, in particular for σ_2. The two cylindrical σ sheets are repeated in the right part of Fig. 4 to emphasize this anisotropy more clearly.

FIG. 4. (Color) Electron-phonon mass enhancement parameter λ at the Fermi surface of MgB_2. The wave vectors are in units of $2\pi/a$. The two inner cylindrical sheets ($\pi_{1,2}$) are given on the right side for clarity.

mesh of **q** points, giving rise to 29 points in the irreducible BZ. The electron wave functions were calculated on a denser, i.e., G_{16}, **k** point grid in the self-consistent solution of the Sternheimer equation. For the *ep* calculation we employed even a G_{40} grid for both the electron and phonon wave vectors by using the exact solution of the Kohn-Sham equation for the former, and the interpolation scheme for the latter. Our phonon dispersion is in good agreement with neutron-scattering measurements[26] and previous calculations.[27]

As Fig. 5 shows, the Fermi surface, consisting of several sheets, is quite complex. Like in the previous example, we indicate the *ep* parameter λ by the color code. The anisotropy of the electron-phonon interaction is not very pronounced in any of the sheets but the strength varies substantially between them. This fact is expressed by the sensitivity of the Eliashberg function to the electron wave vector **k**, as depicted in Fig. 6. While it exhibits very similar features along the ΓH direction on two different sheets (points **a** and **c**) with a double peak between 15 and 25 meV, and a single peak around 27 meV, the behavior is quite different at points **b** and **d**. Here the features below 25 meV are less resolved with a magnitude more than twice in **d** compared to **b**. Figure 7 finally shows the Eliashberg function averaged over the Fermi surface. The so-obtained overall *ep* parameter of λ =0.27 is consistent with existing data from tunneling experiments (see Ref. 8 and references therein).

C. Hydrogen terminated 1×1 W(110) surface

This surface has been extensively studied by means of photoemission measurements aimed to reveal the electronic structure and the effect of electron-phonon interaction on quasiparticle states.[5,28,29] Spin-resolved photoemission[29] showed that the surface state around the high-symmetry point $\bar{S}$ experiences spin-orbit splitting together with an intriguing quasiparticle band splitting that could clearly be attributed to electron-phonon coupling. Here we present results for the paramagnetic surface, i.e., we neglect the effect of the spin-orbit interaction on the surface states. This is justified by the fact that the degenerate paramagnetic Fermi-surface state resembles approximately the spin-split state S_1.[5]

We applied the repeated-slab approach to this system, considering a centrosymmetric supercell, which consists of seven W layers together with two hydrogen surface layers (one on each W surface), and a vacuum thickness equivalent to four ideal W(110) layers. Norm-conserving pseudopotentials with a cut-off energy of 40 Ry were employed. Exchange and correlation effects were treated within the local-density approximation (LDA), utilizing the parametrization by Perdew and Zunger. The surface was considered to be relaxed when the forces acting on each atom were smaller than 10^{-5} Ry/a.u. Our ground-state results are in good agreement with previous all-electron full-potential calculations in terms of the crystal structure as well as the Fermi surface.[30] These calculations revealed a reduced symmetry
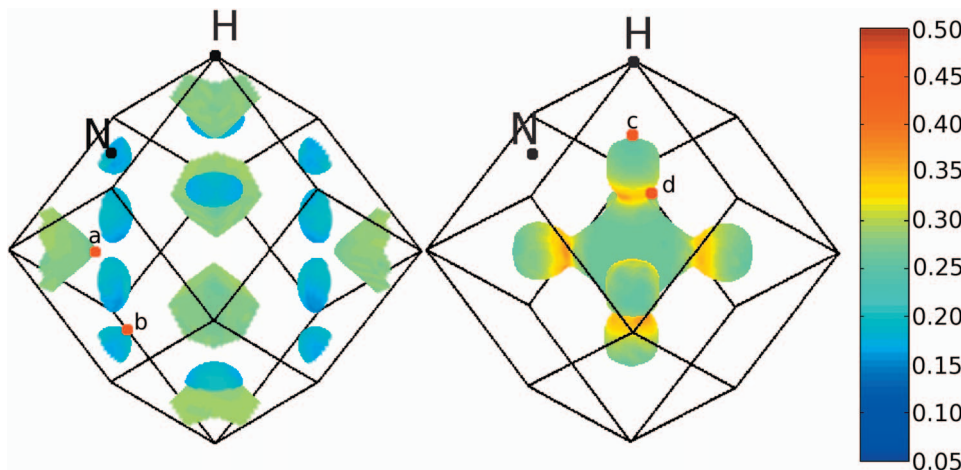

FIG. 5. (Color) Fermi surface of bcc tungsten with the electron-phonon parameter λ highlighted by the color code. The red dots labeled a–d represent selected points for which the Eliashberg function is shown in Fig. 6.
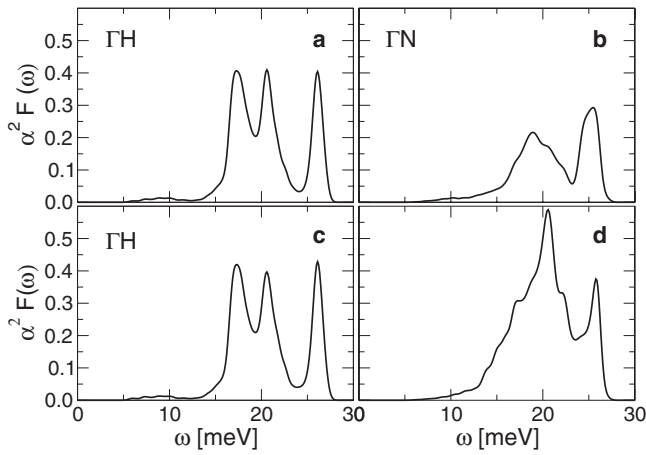
FIG. 6. Eliashberg function for selected points of the Fermi surface, which are indicated by red dots in Fig. 8.

for the relaxed structure with respect to the clean W(110) surface. Figure 8 shows the calculated Fermi surface of the slab system, consisting of electron bands of bulk as well as surface character, where the gray area represents the bulk projected bands.

The best experimentally studied surface electron state is the one around the $\overline{S}$ high-symmetry point (denoted by S surface state in the following), which is indicated by an arrow in Fig. 8. ϑ denotes the angle between a **k** point at the Fermi surface and the high-symmetry line $\overline{HS}$. The whole surface electron band appears almost completely degenerate. There is only a small area where the surface state intersects the bulk projected band area (gray) where the surface state exhibits a tiny splitting due to the finite size of the slab. Hence the size of the slab can be considered sufficiently large to simulate the real surface. The same conclusion can be drawn from checking the degeneracy of the phonon modes in Fig. 9.

A self-consistent linear-response calculation was performed for a uniform $8 \times 8 \times 1$ **q** grid containing 21 irreducible **q** points where for each **q** point, we sampled the electron wave vectors by a $16 \times 16 \times 1$ **k** mesh. Figure 9 shows the so-obtained phonon band structure. The three vibrational modes highest in energy are related to the hydrogen atom displacements while the lower ones are stemming from the
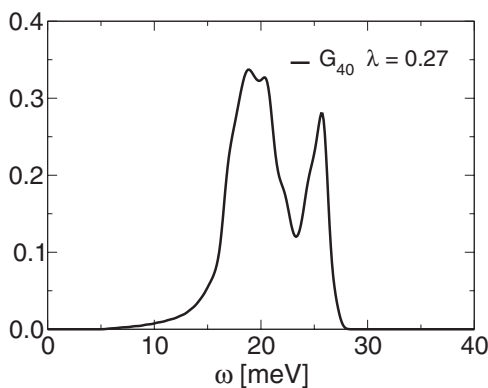

FIG. 7. Eliashberg function averaged over the Fermi surface leading to an overall *ep* parameter λ of 0.27.
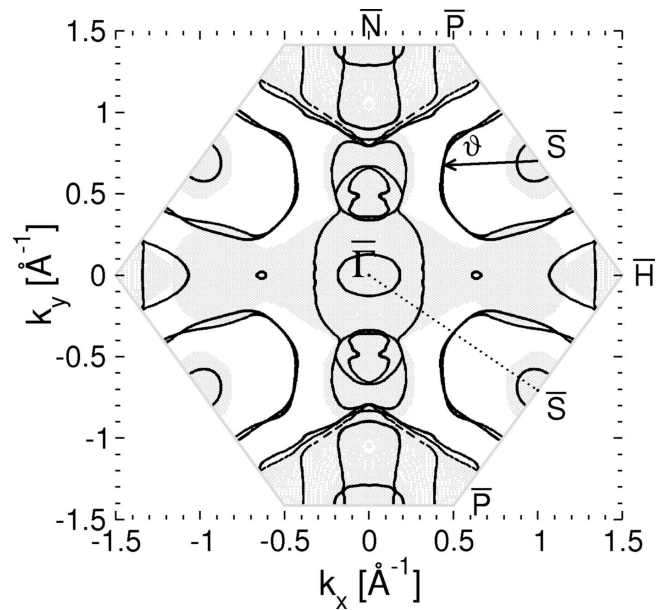

FIG. 8. Fermi surface of the relaxed hydrogen covered W(110) surface system. The gray area indicates the bulk projected bands. The surface electron state S is indicated by the arrow where the angle ϑ is measured from the $\overline{HS}$ line.

underlying W(110) substrate. The mode highest in energy represents ionic motions perpendicular to the surface while the next two lower ones correspond mainly to shear and longitudinal vibrations, respectively. The energies of the hydrogen modes are in very good agreement with low electron energy-loss spectroscopy (EELS) measurements.[31]

With the above results as an input, we resolved the **k** dependency of the Eliashberg function like in the previous sections. We generated the variation of the electron potentials by our interpolation scheme for a uniform $32 \times 32 \times 1$ **q** mesh while the electron wave functions where obtained for
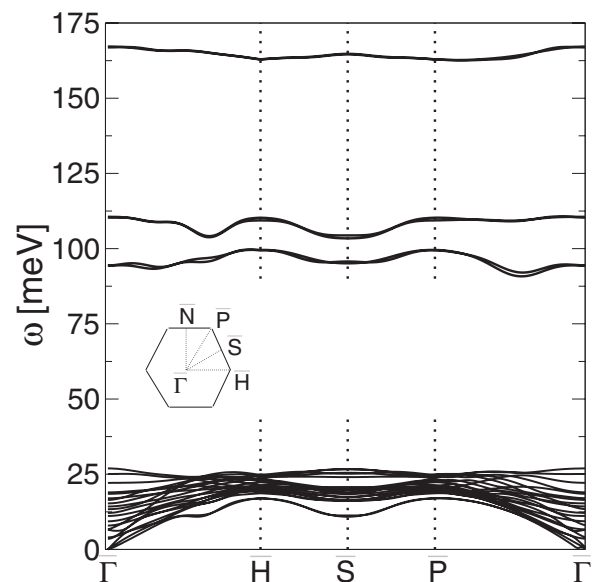

FIG. 9. Phonon dispersion of the hydrogen covered W(110) surface along high-symmetry lines.
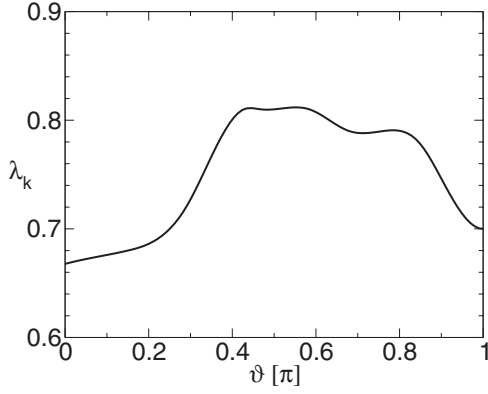
FIG. 10. Dependence of the *ep* interaction λ parameter on the angle ϑ as defined in Fig. 8 for the surface state *S*.

the same grid from the self-consistent potential. The results are shown in Figs. 10 and 11, where the angular dependence of $\lambda_\mathbf{k}$ and the Eliashberg function are depicted, respectively.

Figure 11 shows the calculated Eliashberg function of the *S* surface state for several **k** points in the Fermi surface. The electron wave vector is expressed by the angle ϑ. The dashed green line indicates the first moment of the Eliashberg function, $\int_0^\omega 2\alpha^2 F(\mu)/\mu \, d\mu$, emphasizing the relative importance of specific phonon modes to the total λ parameter. From this figure we deduce that only ~20% of the total mass enhancement is induced by hydrogen related phonons. The relatively weak contribution of the hydrogen surface phonon modes to the total λ parameter is mainly due to the high energies of these phonon states, as they are weighted by the inverse of the frequency. We conclude also that the lowest-energy hydrogen modes, which exhibit the strongest interaction with the surface state, are those with appreciable longitudinal components. In contrast, the high-energy hydrogen vibrations, mostly polarized in the direction perpendicular to the surface, only weakly interact with the surface states.

IV. CONCLUSIONS

In conclusion, we have presented a scheme to accurately describe phonon-induced electron potentials for arbitrary phonon wave vectors. The method is based on the evaluation of the Wannier-function counterpart of the electron potential change and offers the possibility to determine anisotropic properties of the electron-phonon interaction with a computational cost several orders of magnitude less demanding than a fully self-consistent linear-response calculation. To demonstrate the applicability to various examples, we have considered several nontrivial systems, which are bulk MgB_2 and tungsten, and the 1×1 H covered W(110) surface. In all systems, the details of the *ep* interaction at the Fermi surface are revealed by the anisotropic *ep* coupling parameter $\lambda_\mathbf{k}$, as well as by the Eliashberg function. Our results for bulk MgB_2 could also contribute in clarifying the present controversy about the actual value of the Fermi-surface averaged *ep* parameter λ since the present calculation is based on very
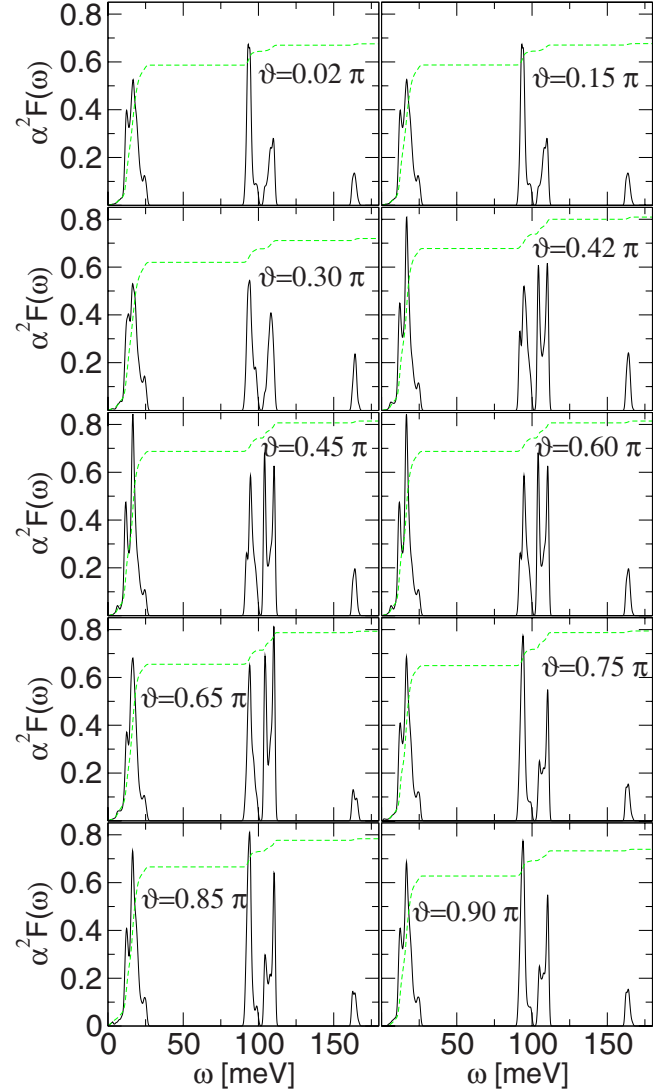

FIG. 11. (Color online) Angular dependence of the Eliashberg function of the surface state *S*. (The definition of ϑ is given in Fig. 8).

dense electron and phonon wave vector samplings. Generally, the evaluation of properties related to *ep* interaction is especially expensive for slab systems. Note that for the particular surface system chosen here, the amount of **q** points considered in the evaluation of the anisotropic Eliashberg function would make a self-consistent calculation of all the phonon-induced changes of the electron potential impracticable.

[1] T. Balasubramanian, E. Jensen, X. L. Wu, and S. L. Hulbert, Phys. Rev. B **57**, R6866 (1998).

[2] S. LaShell, E. Jensen, and T. Balasubramanian, Phys. Rev. B **61**, 2371 (2000).

[3] E. Plummer, J. Shi, S.-J. Tang, E. Rotenberg, and S. Kevan, Prog. Surf. Sci. **74**, 251 (2003).

[4] J. Shi *et al.*, Phys. Rev. Lett. **92**, 186401 (2004).

[5] E. Rotenberg, J. Schaefer, and S. D. Kevan, Phys. Rev. Lett. **84**, 2925 (2000).

[6] A. Eiguren, B. Hellsing, F. Reinert, G. Nicolay, E. V. Chulkov, V. M. Silkin, S. Hufner, and P. M. Echenique, Phys. Rev. Lett. **88**, 066805 (2002).

[7] B. K. Bhattacharyya and J. C. Swihart, J. Phys. F: Met. Phys. **14**, 1651 (1984).

[8] G. Grimvall, *The Electron-Phonon Interaction in Metals* (North-Holland, Amsterdam, 1981).

[9] G. D. Mahan, *Many-Particle Physics* (Plenum, New York, 1990).

[10] S. Y. Savrasov and D. Y. Savrasov, Phys. Rev. B **54**, 16487 (1996).

[11] H. J. Choi, D. Roundy, H. Sun, M. L. Cohen, and S. G. Louie, Phys. Rev. B **66**, 020513(R) (2002).

[12] F. Giustino, Jonathan R. Yates, I. Souza, M. L. Cohen, and G. Louie, Phys. Rev. Lett. **98**, 047005 (2007).

[13] F. Giustino, M. L. Cohen, and S. G. Louie, Phys. Rev. B **76**, 165108 (2007).

[14] I. Souza, N. Marzari, and D. Vanderbilt, Phys. Rev. B **65**, 035109 (2001).

[15] C.-H. Park, F. Giustino, M. L. Cohen, and S. G. Louie, Phys. Rev. Lett. **99**, 086804 (2007).

[16] S. Baroni, S. de Gironcoli, A. D. Corso, and P. Giannozzi, Rev. Mod. Phys. **73**, 515 (2001).

[17] X. Gonze, Phys. Rev. B **55**, 10337 (1997).

[18] R. Kouba, A. Taga, C. Ambrosch-Draxl, L. Nordstrom, and B. Johansson, Phys. Rev. B **64**, 184306 (2001).

[19] A. Eiguren, C. Ambrosch, and P. M. Echenique (unpublished).

[20] J. Nagamatsu, N. Nakagawa, T. Muranaka, Y. Zenitani, and J. Akimitsu, Nature (London) **210**, 63 (2001).

[21] J. Tang, L.-C. Qin, A. Matsushita, Y. Takano, K. Togano, H. Kito, and H. Ihara, Phys. Rev. B **64**, 132509 (2001).

[22] K.-P. Bohnen, R. Heid, and B. Renker, Phys. Rev. Lett. **86**, 5771 (2001).

[23] A. Shukla *et al.*, Phys. Rev. Lett. **90**, 095506 (2003).

[24] A. Y. Liu, I. I. Mazin, and J. Kortus, Phys. Rev. Lett. **87**, 087005 (2001).

[25] Y. Kong, O. V. Dolgov, O. Jepsen, and O. K. Andersen, Phys. Rev. B **64**, 020501(R) (2001).

[26] V. B. Jani and A. R. Gohel, J. Phys. F: Met. Phys. **5**, L25 (1976).

[27] K. Einarsdotter, B. Sadigh, G. Grimvall, and V. Ozolins, Phys. Rev. Lett. **79**, 2073 (1997).

[28] E. Rotenberg and S. D. Kevanb, J. Electron Spectrosc. Relat. Phenom. **126**, 125 (2002).

[29] M. Hochstrasser, J. G. Tobin, E. Rotenberg, and S. D. Kevan, Phys. Rev. Lett. **89**, 216802 (2002).

[30] B. Kohler, P. Ruggerone, and M. Scheffler, Phys. Rev. B **56**, 13503 (1997).

[31] M. Balden, S. Lehwald, H. Ibach, and D. L. Mills, Phys. Rev. Lett. **73**, 854 (1994).